



New Pliocene–Pleistocene $^{40}\text{Ar}/^{39}\text{Ar}$ ages fill in temporal gaps in the Nicaraguan volcanic record

Ian Saginor^{a,*}, Esteban Gazel^b, Michael J. Carr^c, Carl C. Swisher III^c, Brent Turrin^c

^a Division of Natural Sciences and Mathematics, Keystone College, Capwell Hall, La Plume, PA 18440, United States

^b Lamont-Doherty Earth Observatory, Columbia University, 61 Route 9W, Palisades, NY 10964, United States

^c Department of Earth and Planetary Sciences, Rutgers University, 610 Taylor Rd., Piscataway, NJ 08854-8066, United States

ARTICLE INFO

Article history:

Received 16 July 2010

Accepted 12 February 2011

Available online 25 February 2011

Keywords:

Central America
Nicaragua
subduction zone
carbonate crash
geochronology

ABSTRACT

The volcanic record of western Nicaragua documents a significant lull in volcanic activity that has persisted from the late Miocene (~7 Ma) to the formation of the modern volcanic front around 350 ka. This study fills this gap for the first time with samples collected in Northwest Nicaragua between Cosigüina and San Cristóbal volcanoes and with samples collected from the Nicaraguan Depression. We found two previously unknown volcanic units ranging from 3.6 to 1.3 Ma and the improved volcanic record allows us to reconstruct the geochemical evolution of the Nicaraguan arc. U/Th values increased by nearly threefold since the Miocene following the “carbonate crash” at 10 Ma, when dominantly carbonate sediment deposition shifted toward hemipelagic sediment deposition. This transition was thought to be abrupt, however our new data show that it took place gradually over the last 7 Ma. Northwest Nicaragua is a particularly interesting case study because it contains Middle Miocene volcanism on either side of the Nicaraguan Depression, the Coyo Formation (25–7 Ma) to the East and the Tamarindo Formation (14.7–11.7 Ma) to the West. The presence of Mid Miocene volcanism on either side of the Nicaraguan Depression has led to the hypothesis that the two coeval units, currently separated by ~100 km, were once connected and have since been separated by extension. Here, we present data suggesting that the Tamarindo and Coyo are geochemically distinct and therefore cannot be considered part of the same unit.

© 2011 Elsevier B.V. All rights reserved.

1. Introduction

The Central American volcanic front extends 1100 km from the border between Mexico and Guatemala to Costa Rica (Fig. 1) and is generated by the northeasterly subduction of the Cocos Plate underneath the Caribbean Plate. The rate of subduction ranges from 6 cm/yr off southern Guatemala to 9 cm/yr off southern Costa Rica (Demets, 2001).

One of the most obvious arc-wide features in Central America is the physical segmentation of the arc into seven right stepping sections that vary in length from 100 to 300 km (Carr, 1984). The spacing of volcanoes within segments appears to be random with an average of 27 km, however there are a few along-arc gaps with the longest occurring between Cosigüina and San Cristóbal volcanoes in Nicaragua (Fig. 2A and B), a distance of about 80 km. Although there is no active volcanism in this area, topography visible in satellite imagery motivated the present study of that area, which yielded two previously unknown Pliocene to Pleistocene volcanic units.

Ehrenborg (1996) described Middle Tertiary to Recent volcanism of Nicaragua. During the Oligocene, rhyolite shield volcanism resulted in the formation of the Highland Ignimbrites (The word “Tertiary” is used in this paper only in reference to previously published works where it has appeared. The most recent International Stratigraphic Chart does not include this word.). This was followed by basaltic to andesitic Miocene magmas of the Coyo Group. The Coyo Group records fairly continuous volcanic production migrating towards the southwest for at least 60 km before volcanism abruptly stopped ~7 Ma (present paper; Ehrenborg, 1996; Elming et al., 2001; Plank et al., 2002; Carr et al., 2007).

At least 20 km separates the westernmost lavas of the Coyo Group from the modern arc, with the area between them dominated by low-lying topography broken only by minor volcanism intermingled with weathered volcanoclastic sediments. This area is known as the Nicaraguan Depression and contains the country's two largest lakes, Lake Managua and Lake Nicaragua. There is a disagreement (discussed in detail later in this paper) about the depth and total extension of the Nicaraguan Depression, which appears in satellite imagery as an area of low topography between the active front and Miocene volcanism (Weyl, 1980; Weinberg, 1992; van Wyk de Vries, 1993; Morgan et al., 2008).

Widespread volcanism does not appear to have resumed until ~350 ka, with the formation of the present volcanic arc front (Carr

* Corresponding author. Tel.: +1 570 445 8411.

E-mail address: ian.saginer@keystone.edu (I. Saginor).

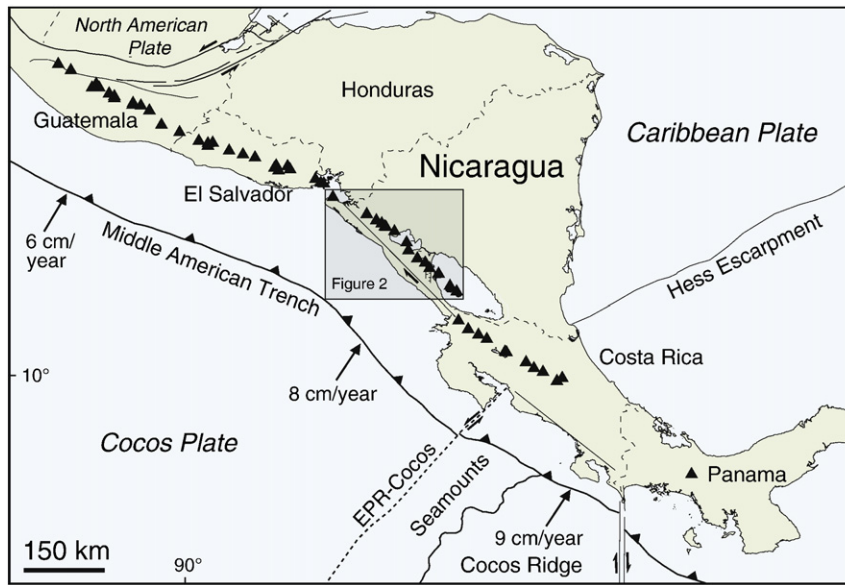


Fig. 1. Map of Central American Volcanic Front. Triangles are Holocene volcanoes.

et al., 2007). Because the tectonic implications of a 7 Ma lull in volcanism along an active arc are large, it was important to be certain that this temporal gap truly existed or if it was merely a product of incomplete sampling. The main purpose of this study was to locate and analyze samples that erupted in western Nicaragua between the

end of Coyal volcanism at 7 Ma and the onset of modern front volcanism at 350 ka. We attempt to at least partially fill in the gap in extrusive volcanism by focusing on samples collected from two distinct areas that have received little attention until now. The first area is between San Cristóbal and Cosigüina and the second is

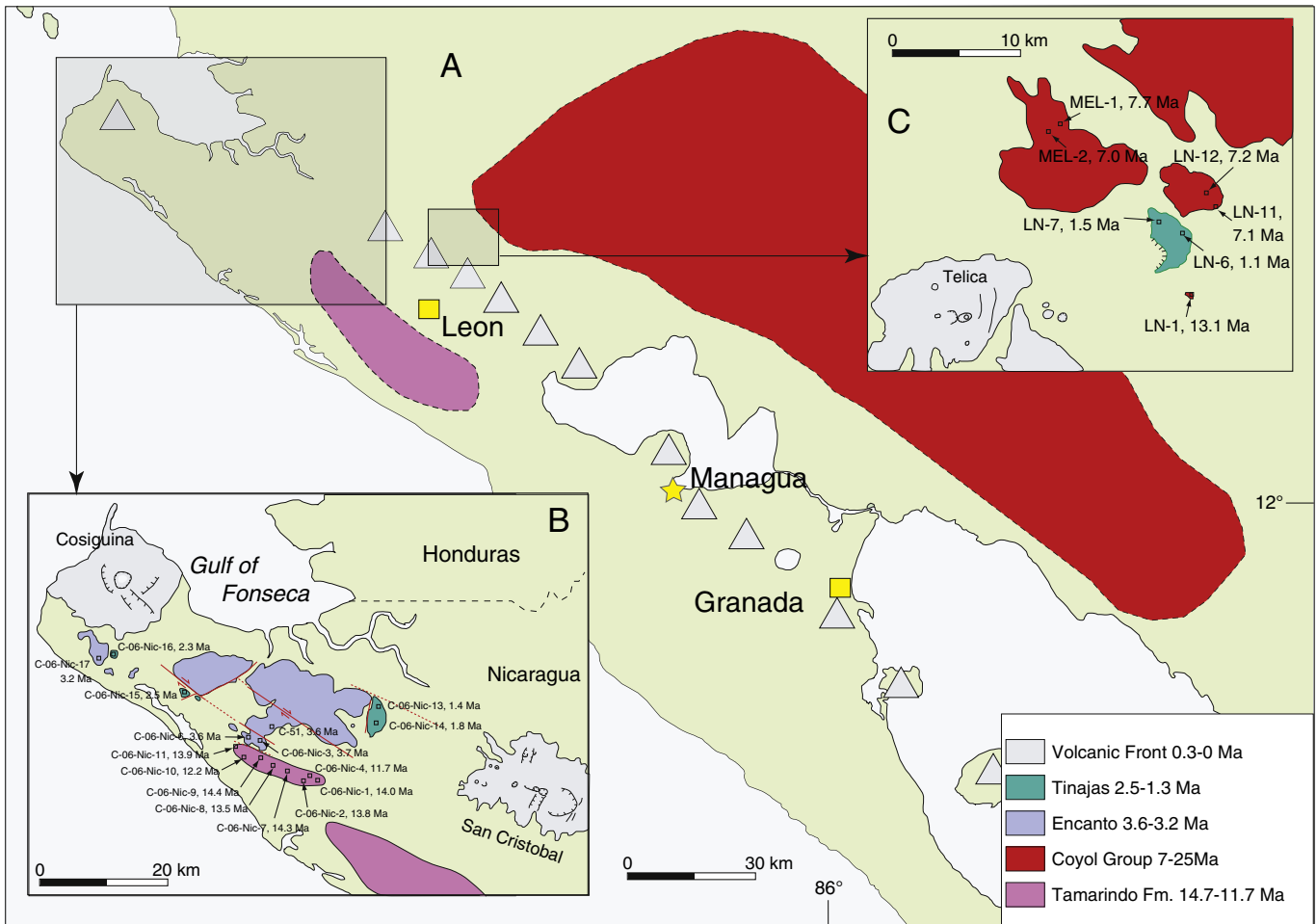


Fig. 2. A) Map of northwest Nicaragua. B) Map of area between Cosigüina and San Cristóbal volcanoes. C) Map of area between volcanic front and Coyal.

between the active front and the Coyo Group on the opposite side of the Nicaraguan Depression.

2. Geologic setting

Lava and tephra samples reported in this study were collected primarily from two areas in western Nicaragua (Fig. 2B and C). The first is located between San Cristóbal and Cosigüina near the northwest termination of the Nicaraguan volcanic front (Fig. 2B). We collected 17 samples from this area, most of which were from a low-lying region of basaltic and andesitic lavas and ignimbrites. This area has not received much prior attention perhaps because it occupies the longest stretch of the Central American Volcanic Front without an active volcano.

McBirney and Williams (1965) described this region as a mix of Quaternary and Tertiary rocks, while the majority of studies list this region as comprising solely Tertiary volcanic material (Weyl, 1980; Nystrom et al., 1988; Darce, 1989; Elming et al., 2001). Also, one early study calls it Quaternary alluvium (Dengo, 1968). The idea that the area was Tertiary was then supported by a single $^{40}\text{Ar}/^{39}\text{Ar}$ date from a sample collected nearby from the Tamarindo Formation (Elming et al., 2001).

The second primary area of study is shown in Fig. 2C and is located between the Coyo Group and the active volcanic front. This area was selected in an attempt to locate material that erupted during an apparent hiatus in volcanic production between the end of Miocene volcanism at 7 Ma and the appearance of the modern arc ~350 ka (Carr et al., 2007). This area consists mainly of weathered hills of basalts to basaltic andesites and volcanoclastic sediments that partially fill in the Nicaraguan Depression. The volcanic features in this area are low-lying, with a maximum relief of only a few hundred meters, although recent sediments may bury additional relief.

Finally, three samples around the Masaya Volcano were also dated. Two (Ban-00-2 and Ban-00-1BM) are lavas taken from the Las Banderas Group northeast of Masaya near the town of Tipitapa and one (LS-00-4) is a tephra from the Las Sierras Group on Masaya's southwestern flank near Diriamba. These samples were chosen, because the Las Sierras and Las Banderas Groups near Masaya were thought to represent the earliest expressions of the active arc in Nicaragua.

The Tamarindo Formation (Fig. 2A and B) consists of a narrow band of basaltic to andesitic lavas interlayered with thick ignimbrite deposits and volcanoclastic sediments that parallel Nicaragua's Pacific coast west of the modern volcanic front. McBirney and Williams (1965) made a more careful description of the area and emphasized the prevalence of ignimbrite deposits over the less common lavas.

Geologic maps of Nicaragua created over the last 40 years have exposed confusion about the origin of the Tamarindo Formation. A 1968 map by Dengo (1968) included parts of the Tamarindo in the active arc and filled in the area between the volcanic front and the Pacific coast with Quaternary alluvium and Tertiary sedimentary rocks. Nystrom et al. (1988) and Elming et al. (2001) list both the Tamarindo and Coyo as "Tertiary volcanic rocks" whereas McBirney and Williams (1965) seem to ignore the lava component of the Tamarindo entirely and label the Tamarindo as Tertiary ignimbrites, despite having noted the presence of interlayered lavas. Weinberg (1992) uses a modified map after a Ph.D. thesis by Darce (1989) and differentiates the Coyo from the Matagalpa Group, the latter being composed primarily of ignimbrites, which surround Coyo deposits on all sides. On this map, the Tamarindo is not listed by name and is included as part of the Matagalpa Group. Weyl (1980) lists the age of Tamarindo variously as Eocene, Oligocene, or Miocene, despite citing a Mid Miocene K–Ar age in the text and is similarly unsure about whether to group the Tamarindo and Coyo together.

Weyl (1980) provided the first K–Ar age constraint for the Tamarindo Formation with a Mid Miocene age of 13.7 ± 0.5 Ma, which, according to Weyl, makes it equivalent in age with the Coyo Formation. This age assignment is supported by four subsequent K–Ar ages for the Tamarindo Formation ranging between 12.3 and 18.4 Ma (Ehrenborg, 1996; Elming et al., 2001; Plank et al., 2002). The upper age limit (18.4 Ma) comes from a whole rock K–Ar analysis on an ignimbrite and may be anomalously old, due to possible xenolith or xenocryst contamination.

3. Methods

Samples for geochemistry and $^{40}\text{Ar}/^{39}\text{Ar}$ dating were obtained from the cores of large boulders or lava blocks collected from the study areas. Most of the samples appear fresh and unweathered despite apparent intense surficial weathering. The samples were observed under binocular and petrographic microscopes and those that showed the least amount of weathering or alteration were prepared for geochemistry and $^{40}\text{Ar}/^{39}\text{Ar}$ dating.

For the $^{40}\text{Ar}/^{39}\text{Ar}$ analyses, matrix (groundmass) and mineral separates were prepared and analyzed following the methods outlined in Carr et al. (2007). The samples were loaded into individual sample wells of aluminum irradiation disks, along with aliquots of the irradiation monitor mineral Alder Creek rhyolite sanidine (AC-1). The loaded sample disks were wrapped in Al foil, sealed in quartz glass tubes, and then irradiated for 0.25 h in the Cadmium-Lined, In-Core Irradiation Tube (CLICIT) facility of the Oregon State University Triga Research Reactor (OSTR).

The irradiated samples were loaded into sample wells in a stainless steel disk, loaded onto the sample extraction line and baked out at ~100 °C overnight. Approximately 80 mg of per sample were incrementally heated in step-wise fashion (15 increments per sample) using a CO₂ laser focused through a 6 mm integrator lens. Released gasses were purified using an internal cold finger to collect water vapor and a C50 getter removed unwanted interference gasses. Ar was measured on a MAP215-50 mass spectrometer using both conventional analog and pulse counting methods. Calibration and determination of the irradiation parameter J was determined by multiple total fusion analyses of the co-irradiated monitor mineral AC-1 using a published reference age of 1.194 ± 0.006 Ma (Turrin et al., 1994; Renne et al., 1998). Interference isotopes produced during irradiation of the samples were corrected using previously published values ($^{36}\text{Ar}/^{37}\text{Ar}$)_{Ca} = $2.72 \pm 0.06 (\times 10^{-4})$, ($^{39}\text{Ar}/^{37}\text{Ar}$)_{Ca} = $7.11 \pm 0.02 (\times 10^{-4})$, ($^{38}\text{Ar}/^{39}\text{Ar}$)_K = $1.22 \pm 0.02 (\times 10^{-2})$, and ($^{40}\text{Ar}/^{39}\text{Ar}$)_K = $7 = 3 (\times 10^{-4})$ (Renne et al., 1998; Deino et al., 2002). During the analysis of the samples and standards, mass discrimination was regularly monitored through measurement of air aliquots delivered via an on-line automated air pipette system and varied between 1.000 and 1.007 AMU. Data reduction was made using software program MassSpec written by A. Deino.

Data are plotted on release spectra that show the apparent age and the percent of released ^{40}Ar of radiogenic origin for each temperature step with plateau steps overlapping at 2 Sigma. $^{36}\text{Ar}/^{40}\text{Ar}$ is also plotted against $^{39}\text{Ar}/^{40}\text{Ar}$ on inverse isochron diagrams. Ideally, the data for each individual step fit on a single line such that the x-intercept provides the age and the y-intercept provides the initial $^{36}\text{Ar}/^{40}\text{Ar}$ value. The scatter about the isochron line is given by the mean squared weighted deviation (MSWD). The data is included in Appendix A and the diagrams in Appendix B.

Samples for major and trace element analysis were powdered using an alumina powdering mill and analyzed by LA-ICP-MS and XRF at Michigan State University according to the methods outlined in Szymanski (2007) and Hannah et al. (2002). Homogeneous glass disks were produced for the samples by fusing each powder (3 g) with a lithium tetraborate (Li₂B₄O₇) flux (9 g); ~0.5 g of ammonium nitrate (NH₄NO₃) was added to ensure oxidation of iron during fusion. Samples were weighed in Pt crucibles (95% Pt, 5% Au) and

Table 1
ICP-MS, XRF, and $^{40}\text{Ar}/^{39}\text{Ar}$ data. Bold indicates preferred age. LOI is calculated by the SPECTRAplus software and not measured. It is calculated assuming that the difference from 100% is lost during fusion.

Unit	C-06-Nic-1	C-06-Nic-2	C-06-Nic-3	C-06-Nic-4	C-06-Nic-5	C-06-Nic-6	C-06-Nic-7	C-06-Nic-8	C-06-Nic-9	C-06-Nic-10
	Tam.	Tam.	Encanto	Tam.		Encanto	Tam.	Tam.	Tam.	Tam.
Easting	475,660	468,539	469,294	469,294	465,859	465,620	464,718	462,685	461,284	458,616
Northing	1,404,776	1,402,932	1,407,569	1,407,569	1,405,433	1,406,257	1,406,210	1,406,665	1,407,499	1,405,529
Dist. along trench	603.6	598.5	596.8	596.8	595	594.3	593.6	591.6	590	588.8
Dist. from trench	178.1	173	177.4	177.4	173.9	174.4	174	173.3	173.4	170.4
Plateau age	14.03 ± 0.05	13.76 ± 0.09	3.653 ± 0.020	11.71 ± 0.05	n/a	3.60 ± 0.03	14.25 ± 0.08	n/a	13.54 ± 0.06	n/a
Total fusion age	14.06 ± 0.07	13.73 ± 0.17	3.59 ± 0.03	11.75 ± 0.07	n/a	3.59 ± 0.03	14.13 ± 0.08	n/a	12.64 ± 0.07	12.22 ± 0.07
Isochron age	14.03 ± 0.13	13.76 ± 0.16	3.68 ± 0.04	11.40 ± 0.17	n/a	3.52 ± 0.09	14.48 ± 0.15	14.4 ± 0.7	13.78 ± 0.17	14.72 ± 0.09
$^{40}\text{Ar}/^{39}\text{Ar}$ int.	294 ± 2	295.5 ± 0.9	294.2 ± 0.8	301 ± 3	n/a	300 ± 5	290.8 ± 1.6	284 ± 18	292 ± 3	227.2 ± 1.9
MSWD	2.1	1.2	2.4	1	n/a	0.4	1.5	0.54	1.3	1.2
% ^{39}Ar on plateau	63	100	93	100	n/a	100	85	n/a	62	n/a
SiO ₂	51.65	n/a	49.42	51.6	51.99	49.35	49.95	56.24	52.94	53.42
TiO ₂	1.13	n/a	0.69	0.56	1.15	0.82	1.02	1.65	1.87	1.71
Al ₂ O ₃	15.61	n/a	20.68	18.37	15.93	17.79	16.19	13.89	13.48	14.27
Fe ₂ O ₃	11.65	n/a	9.23	8.29	11.3	10.97	11.09	11.06	12.97	12.27
MnO	0.17	n/a	0.17	0.15	0.18	0.2	0.21	0.2	0.21	0.21
MgO	4.14	n/a	3.33	4.43	3.68	3.85	5.48	2.94	3.84	3.49
CaO	8.69	n/a	9.98	8.91	8.25	10.3	9.68	7.07	7.95	7.54
Na ₂ O	2.77	n/a	2.83	2.77	2.88	2.36	2.63	2.85	2.58	2.49
K ₂ O	0.7	n/a	0.66	0.38	0.77	0.65	0.39	0.95	0.95	0.93
P ₂ O ₅	0.18	n/a	0.13	0.06	0.21	0.13	0.17	0.35	0.35	0.33
Totals	96.69	n/a	97.12	93.52	96.34	96.42	96.81	97.2	97.14	96.69
LOI	3.17	n/a	2.73	4.36	3.51	3.43	3.06	2.57	2.62	3.08
V	385	n/a	212	220	370	345	378	329	470	400
Ni	29	n/a	33	25	24	21	35	23	31	26
Cu	129	n/a	98	152	357	205	297	318	456	326
Zn	88	n/a	68	61	85	77	79	106	106	110
Rb	12	n/a	9	7	15	9	7	23	20	12
Sr	339	n/a	561	318	356	409	369	341	316	344
Y	28.68	n/a	16.47	17.85	29.64	21.71	23.93	54.68	56.71	53.3
Zr	69	n/a	38	36	78	43	57	153	148	140
Nb	1.09	n/a	0.84	0.57	1.81	0.79	0.97	2.09	1.97	1.92
Ba	518	n/a	583	367	494	533	465	972	945	1004
La	4.41	n/a	4.59	1.96	5.8	3.94	3.95	9.1	8.95	8.46
Ce	10.59	n/a	10.23	5.38	12.53	9.25	9.93	22.22	21.16	19.9
Pr	1.82	n/a	1.57	0.88	2.16	1.52	1.71	3.92	3.88	3.62
Nd	9.79	n/a	7.74	4.87	11.61	8.03	9.12	21.17	21.18	19.57
Sm	3.2	n/a	2.21	1.73	3.57	2.5	2.9	7.04	7.05	6.46
Eu	1.03	n/a	0.84	0.69	1.16	0.86	0.99	2.06	1.97	1.95
Gd	3.54	n/a	3.27	2.08	3.96	2.71	3.13	7.45	7.58	7.19
Tb	0.61	n/a	0.4	0.39	0.68	0.48	0.54	1.26	1.29	1.21
Dy	4.34	n/a	2.52	2.62	4.57	3.27	3.65	8.74	9.08	8.31
Ho	0.86	n/a	0.49	0.54	0.91	0.65	0.73	0.1.75	1.84	1.68
Er	2.58	n/a	1.5	1.67	2.74	1.94	2.24	5.27	5.34	5.07
Yb	2.66	n/a	1.55	1.82	2.84	2.06	2.29	5.62	5.72	5.41
Lu	0.41	n/a	0.24	0.27	0.42	0.31	0.35	0.83	0.83	0.8
Hf	2.15	n/a	1.09	1.1	2.24	1.32	1.73	4.83	4.85	4.56
Ta	0.08	n/a	0.03	0.02	0.12	0.04	0.07	0.16	0.15	0.15
Pb	2.55	n/a	1.83	1.51	2.7	2.31	2.35	5.72	5.68	6.39
Th	0.31	n/a	0.61	0.18	0.4	0.39	0.26	0.73	0.64	0.7
U	0.16	n/a	0.49	0.11	0.19	0.41	0.16	0.42	0.36	0.38
Cr	20	n/a	5	8	9	4	50	2	16	2

suspended over an oxidizing flame (~1000 °C) on an orbital mixing stage for 25 min. Resulting melts were poured into red-hot Pt molds (40 mm diameter) and cooled on a hot plate at ~500 °C. These glass disks were then analyzed for major elements and selected trace elements by X-ray fluorescence (XRF) and for trace elements by laser ablation inductively-coupled plasma mass spectrometry (LA-ICP-MS).

Fused disks were analyzed for major elements (SiO₂, TiO₂, Al₂O₃, Fe₂O₃, MnO, MgO, CaO, Na₂O, K₂O, and P₂O₅) as well as Rb, Sr, and Zr on a Bruker S4 Pioneer XRF. Data were reduced using fundamental parameters (e.g. Criss, 1980) in SPECTRAplus software (Bruker AXS, Germany) on the S4 Pioneer; trace elements were determined using standard linear regression techniques. Precision for most elements is <1% RSD, except for P₂O₅ (<2%).

Trace element concentrations were determined on the same glass disks using a CETAC LSX 200 Plus Nd:YAG (266 nm) laser on a Micromass (now Thermo Electron Corporation) Platform ICP-MS with

hexapole collision cell. Samples were ablated using a single line scan, after a pre-ablation to clean and roughen the surface. A spot size of 250 μm and a 150 μm/s scan rate were used for the pre-ablation, while the ablation for data acquisition used a 200 μm spot size, a scan rate of 10 μm/s and a defocus into the sample of 50 μm. Using the Selected Ion Recording (SIR) function in the MassLynx software (Waters Corporation, U.S.A.) data for twenty-three (23) elements were acquired: V, Cr, Y, Nb, Ba, La, Ce, Pr, Nd, Sm, Eu, Gd, Tb, Dy, Ho, Er, Yb, Lu, Hf, Ta, Pb, Th and U. A set of 12–15 external rock standards, representing a wide variety of igneous rock compositions and prepared using an identical fusion method, was used for calibration. Before processing, the background signal from the Ar/He carrier gas was subtracted from each sample and standard. Strontium (or zirconium), determined by XRF on the same glass disks, was used as the internal standard for quantification. Final concentrations were determined using a standard linear regression for each element (normalized signal vs. concentration), using only standards with

C-06-Nic-11	C-06-Nic-12	C-06-Nic-13	C-06-Nic-14	C-06-Nic-15	C-06-Nic-16	C-06-Nic-17	C-51	Sa-1	MEL-1	MEL-2	LN-1
Tam.		Tinajas	Tinajas	Tinajas	Tinajas	Encanto	Encanto	Coyol	Coyol	Coyol	Coyol
458,102	479,610	477,630	479,875	453,307	439,801	436,857	472,920	544,588	531,139	526,947	541,035
1,405,850	1,415,351	1,419,917	1,413,921	1,417,082	1,422,361	1,421,559	1,408,510	1,422,797	1,405,468	1,403,408	1,394,849
588.2	601.6	597.7	602.6	578.5	564.4	562.3	599.4	653	650.2	647.7	663.9
170.4	189.1	192.1	188.1	177.6	175.5	173.3	180	227.6	206.1	202.3	201.9
13.90 ± 0.07	n/a	1.364 ± 0.009	1.770 ± 0.017	2.49 ± 0.03	2.34 ± 0.03	3.181 ± 0.011	3.590 ± 0.03	8.89 ± 0.07	7.72 ± 0.02	6.95 ± 0.03	13.151 ± 0.017
12.84 ± 0.06	n/a	1.359 ± 0.013	1.85 ± 0.04	2.46 ± 0.03	2.25 ± 0.03	3.09 ± 0.02	3.550 ± 0.04	9.54 ± 0.19	7.66 ± 0.03	6.86 ± 0.10	13.03 ± 0.04
14.4 ± 0.3	n/a	1.364 ± 0.011	1.64 ± 0.06	2.66 ± 0.07	2.45 ± 0.03	3.196 ± 0.015	3.640 ± 0.05	8.3 ± 0.3	7.82 ± 0.13	7.5 ± 0.3	13.11 ± 0.10
285.5 ± 5	n/a	295 ± 6	299.7 ± 1.3	292.5 ± 1.0	251 ± 6	290.6 ± 0.7	294 ± 0.8	301.0 ± 0.7	291 ± 13	285 ± 2	295 ± 2
0.78	n/a	0.5	2.9	0.2	0.17	1.2	1	1.1	4.7	1.2	6.8
62	n/a	100	61	93	87	86	98	60	62	92	80
55.14	76.98	57.75	58.69	50.05	55.42	58.99	47.14	49.38	51.37	60.54	55.99
1.74	0.23	0.6	0.62	0.94	0.68	0.64	0.74	0.83	0.74	0.69	0.82
13.93	10.65	16.94	15.76	17.37	19.12	16.25	20.43	17.16	16.75	16.73	17.48
11.53	2.4	6.85	6.98	10.51	6.96	7.87	10.06	9.98	8.95	4.84	6.76
0.21	0.04	0.1	0.13	0.19	0.11	0.14	0.17	0.21	0.21	0.26	0.13
3.22	0.48	2.87	2.78	4.26	1.94	2.11	3.92	6.23	4.61	1.48	1.97
7.44	1.05	6.99	6.51	9.18	7.67	6.06	11.49	1.06	9.49	5.33	6.42
2.76	2.56	2.82	2.92	2.9	3.06	3.33	2.23	2.58	2.56	3.39	3.47
0.93	1.22	1.3	1.35	0.67	1.4	1.05	0.47	0.61	1.32	2.44	1.95
0.34	0.33	0.1	0.13	0.24	0.17	0.13	0.1	0.22	0.17	0.25	0.21
97.24	95.94	96.32	95.87	96.31	96.53	96.57	96.75	97.22	96.17	95.95	95.2
97.24	3.92	3.52	3.97	3.53	3.3	3.25	3.11	2.64	3.63	3.82	4.67
386	50	266	207	305	170	169	288	277	249	102	144
26	16	20	17	25	18	24	21	55	33	18	19
415	51	39	77	104	116	171	336	92	121	47	44
108	29	62	55	88	60	66	67	71	76	58	63
22	15	23	22	14	28	19	7	7	34	70	39
340	162	361	366	478	396	340	518	494	477	404	354
56.31	15.15	20.54	22.98	25.58	26.64	33.33	16.9	18.69	24.6	32.97	26.26
144	96	81	96	64	99	86	29	55	85	175	140
1.96	1.71	1.23	1.6	1.21	1.36	1.22	0.64	1.67	1.65	3.53	2.98
942	1188	996	1033	654	918	875	438	429	865	1634	523
9.06	9.29	6.14	7.5	7.74	8.94	6.7	3.62	6.83	8.9	13.71	10.39
21.34	14.48	14.44	17.96	18.1	17.98	14.23	7.86	15.63	17.98	30.07	22.57
3.77	2.23	2.07	2.43	2.76	2.84	2.49	1.27	2.19	2.84	4.28	3.17
20.34	8.86	9.48	11.15	13.65	13.01	12.78	6.59	10.38	13.75	18.85	14.41
6.68	2.06	2.75	3.03	3.73	3.48	3.9	2.04	2.76	3.62	4.91	3.73
1.99	0.72	0.87	0.94	0.1.17	1.06	1.12	0.76	0.95	1.06	1.3	1.06
7.36	2.2	2.89	3.19	3.82	3.78	4.18	2.28	2.92	3.73	4.88	3.87
1.24	0.37	0.47	0.51	0.6	0.61	0.7	0.4	0.47	0.6	0.78	0.64
8.82	1.99	2.84	3.15	3.82	3.74	4.68	2.58	2.78	3.71	4.7	3.87
1.74	0.4	0.57	0.65	0.75	0.74	0.94	0.52	0.54	0.73	0.92	0.75
5.21	1.28	1.74	2	2.22	2.2	2.86	1.57	1.67	2.13	2.79	2.23
5.45	1.41	1.9	2.13	2.32	2.32	2.98	1.57	1.66	2.28	2.93	2.31
0.82	0.24	0.29	0.33	0.34	0.36	0.47	0.24	0.26	0.34	0.44	0.36
4.7	2.4	2	2.33	1.67	2.61	2.44	1.01	1.3	2.39	4.3	3.4
0.15	1.21	0.05	0.06	0.04	0.11	0.12	0.02	0.06	0.11	0.38	0.23
5.76	5.21	3.47	3.75	3.78	5.77	3.41	3.97	2.75	6.43	12.38	5.66
0.72	1.67	1.03	1.11	0.69	1.28	0.83	0.5	0.39	1.42	2.57	1.98
0.38	3.77	1.33	1.25	0.71	1.19	0.56	0.32	0.27	0.67	1.61	0.85
2	2	14	6	35	2	1	3	132	23	2	2

calculated values within 15% of preferred, published values. Precision for all elements is <5% RSD.

4. Data and results

Twenty one new major and trace-element geochemical analyses and twenty nine new $^{40}\text{Ar}/^{39}\text{Ar}$ analyses are presented in this paper (Table 1). Samples generally plot along the calc-alkaline series and range from basalt to andesite in composition (Fig. 3), although some less common dacites were also found.

The area between San Cristóbal and Cosigüina yielded sixteen $^{40}\text{Ar}/^{39}\text{Ar}$ dates and seventeen geochemical analyses. As mentioned earlier, the age of material from this area was not known, however it has been generally assumed to consist of a single unit. Our data reveal three geochemically and morphologically distinct units spanning at least 13 Ma ranging from 1.1 to 14.3 Ma. The first unit is identified as the northwestern terminus of the Tamarindo Formation. The other

two do not fit into the current stratigraphy of western Nicaragua making it is necessary to name and define these two previously unknown units.

4.1. Tamarindo Formation

The Tamarindo Formation has been studied before, but was never thought to extend this far to the northwest (Plank et al., 2002) (Fig. 2A and B). Eight lavas and one tephra were collected and analyzed from the Tamarindo Formation producing eight $^{40}\text{Ar}/^{39}\text{Ar}$ dates and eight geochemical analyses. Chondrite normalized Rare Earth Element (REE) patterns for these samples are flat (Fig. 4) with La/Yb values between 1 and 2 (Fig. 8) and are consistent with previously published values for the Tamarindo Formation (Plank et al., 2002). Although all Tamarindo samples show similar REE patterns, four of these samples have distinctly elevated REE (up to 40 times chondritic, Fig. 4) and TiO_2 values (>1 wt.%, not shown).

Table 1 (continued)

Unit	LN-6	LN-7	LN-11	LN-12	Ban-00-2	Ban-00-1BM	Bal-8	Bal-10	LS-00-4
	Tinajas	Tinajas	Coyol	Coyol	Tinajas	Tinajas			Tinajas
Easting	543,354	542,503	544,873	544,670	61,368	61,263	3,916,464	3,808,123	56,119
Northing	1,401,672	1,402,188	1,405,051	1,405,510	136,236	13,621	14,610,376	1,461,636	131,557
Dist. along trench	662.5	661.5	662.1	661.7	741.7	741	504.3	494.8	720.7
Dist. from trench	208.9	209	212.6	212.9	210	209.3	184.9	180	144
Plateau age	1.13 ± 0.05	1.48 ± 0.02	7.188 ± 0.006	7.111 ± 0.008	1.24 ± 0.03	1.3 ± 0.03	1.067 ± 0.011	0.974 ± 0.017	1.749 ± 0.018
Total fusion age	1.06 ± 0.04	1.47 ± 0.04	7.098 ± 0.008	7.060 ± 0.010	1.25 ± 0.03	1.29 ± 0.03	1.061 ± 0.014	1.057 ± 0.013	1.75 ± 0.02
Isochron age	1.56 ± 0.15	1.48 ± 0.06	7.19 ± 0.03	7.12 ± 0.03	1.21 ± 0.08	1.3 ± 0.2	1.09 ± 0.04	1.11 ± 0.06	1.68 ± 0.05
⁴⁰ Ar/ ³⁶ Ar int.	286 ± 3	295 ± 1.9	293 ± 3	294 ± 2	297 ± 4	300 ± 20	292 ± 3	273 ± 15	303 ± 6
MSWD	1	1.4	5	4	0.41	0.38	2.4	1.1	1
% ³⁹ Ar on plateau	93	100	87	78	100	100	73	78	100
SiO ₂	57.61	55.52	67.06	67.12	n/a	n/a	n/a	n/a	n/a
TiO ₂	0.7	0.71	0.55	0.54	n/a	n/a	n/a	n/a	n/a
Al ₂ O ₃	17.05	17.74	14.63	14.93	n/a	n/a	n/a	n/a	n/a
Fe ₂ O ₃	7.52	8.4	4.04	4.02	n/a	n/a	n/a	n/a	n/a
MnO	0.18	0.17	0.06	0.05	n/a	n/a	n/a	n/a	n/a
MgO	2.38	2.54	0.59	0.54	n/a	n/a	n/a	n/a	n/a
CaO	5.78	6.92	3.16	3.13	n/a	n/a	n/a	n/a	n/a
Na ₂ O	3.73	3.63	4.31	4.31	n/a	n/a	n/a	n/a	n/a
K ₂ O	1.07	0.79	2.12	2.11	n/a	n/a	n/a	n/a	n/a
P ₂ O ₅	0.19	0.22	0.14	0.14	n/a	n/a	n/a	n/a	n/a
Totals	96.21	96.64	96.66	96.89	n/a	n/a	n/a	n/a	n/a
LOI	3.62	3.17	3.13	2.91	n/a	n/a	n/a	n/a	n/a
V	115	182	109	112	n/a	n/a	n/a	n/a	n/a
Ni	20	19	32	18	n/a	n/a	n/a	n/a	n/a
Cu	47	167	232	73	n/a	n/a	n/a	n/a	n/a
Zn	83	74	50	51	n/a	n/a	n/a	n/a	n/a
Rb	13	9	38	39	n/a	n/a	n/a	n/a	n/a
Sr	467	539	278	288	n/a	n/a	n/a	n/a	n/a
Y	29.44	42.69	34.47	79.67	n/a	n/a	n/a	n/a	n/a
Zr	55	47	166	165	n/a	n/a	n/a	n/a	n/a
Nb	1.17	1.25	4.09	4.12	n/a	n/a	n/a	n/a	n/a
Ba	984	807	1348	1347	n/a	n/a	n/a	n/a	n/a
La	7.89	11.96	13.92	32.16	n/a	n/a	n/a	n/a	n/a
Ce	14.62	19.58	29.34	49.45	n/a	n/a	n/a	n/a	n/a
Pr	2.44	4.31	3.9	8.97	n/a	n/a	n/a	n/a	n/a
Nd	12.25	21.98	16.6	39	n/a	n/a	n/a	n/a	n/a
Sm	3.5	6.07	4.18	9.27	n/a	n/a	n/a	n/a	n/a
Eu	1.23	2.2	1.17	2.75	n/a	n/a	n/a	n/a	n/a
Gd	3.67	6.16	4.41	9.8	n/a	n/a	n/a	n/a	n/a
Tb	0.6	0.96	0.72	1.39	n/a	n/a	n/a	n/a	n/a
Dy	3.86	6.44	4.25	9.09	n/a	n/a	n/a	n/a	n/a
Ho	0.76	1.23	0.87	1.82	n/a	n/a	n/a	n/a	n/a
Er	2.31	3.59	2.68	5.41	n/a	n/a	n/a	n/a	n/a
Yb	2.44	3.88	2.95	5.86	n/a	n/a	n/a	n/a	n/a
Lu	0.38	0.55	0.45	0.88	n/a	n/a	n/a	n/a	n/a
Hf	1.64	1.33	3.26	3.3	n/a	n/a	n/a	n/a	n/a
Ta	0.08	0.1	0.54	0.59	n/a	n/a	n/a	n/a	n/a
Pb	4.07	2.48	9.38	9.77	n/a	n/a	n/a	n/a	n/a
Th	0.54	0.51	1.91	1.91	n/a	n/a	n/a	n/a	n/a
U	0.58	0.85	1.64	1.84	n/a	n/a	n/a	n/a	n/a
Cr	1	3	3	3	n/a	n/a	n/a	n/a	n/a

⁴⁰Ar/³⁹Ar ages on these samples range from 13.8 to 14.7 Ma with one sample significantly younger with an age of 11.7 Ma.

4.2. Coyol Group

Six samples collected from the low lying area just behind the active arc were found to have geochemistry and ages (6.95 to 13.31 Ma) in the range of previously reported data (Plank et al., 2002) from the Coyol Group. The Coyol Group is characterized by relatively steep REE patterns compared to the Tamarindo samples (Fig. 4). Sample LN-1 (13.3 Ma) is contemporaneous to the Tamarindo Formation, but shares a geochemical affinity to Coyol (relatively steep REE patterns).

4.3. Encanto unit

The Encanto unit is named after a small hill (12.7146°N/87.2771°W) located near the first collected sample (C-51) and

makes up the bulk of volcanic material between San Cristóbal and Cosigüina. Characterized by low-lying heavily weathered hills, it is also found on the southern flank of Cosigüina ~3 km from the coast. Chondrite normalized REE patterns are slightly steeper than Tamarindo with the LREEs being elevated relative to HREEs (Fig. 4), with La/Yb values between 2 and 3 (Fig. 8).

⁴⁰Ar/³⁹Ar dating of four samples from the Encanto ranged in age from 3.6 to 3.2 Ma (Table 1, Fig. 5, Appendix 2).

4.4. Tinajas unit

This unit is named after one of its characteristic small smooth round hills of basalt (12.7960°N/87.1981°W). The Tinajas unit is a series of isolated hills and distinguishes itself morphologically from the deeply eroded Encanto. REE patterns are slightly steeper than Encanto and significantly steeper than Tamarindo (Fig. 4)

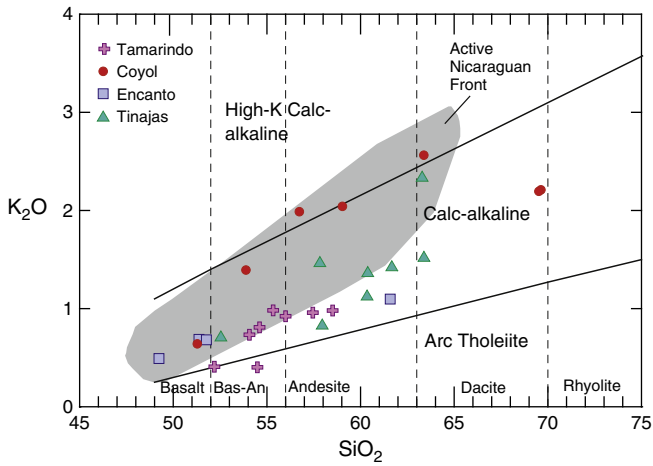


Fig. 3. Rock classification diagram for all analyzed samples (Peccerillo and Taylor, 1976). Purple crosses are Tamarindo, blue squares are Encanto, green triangles are Tinajas, and red circles are the Coyoil Group.

with La/Yb values between 3 and 4 (Fig. 8). This REE pattern is consistent with that of the modern volcanic front.

⁴⁰Ar/³⁹Ar ages for the Tinajas range from 1.3 to 2.5 Ma, with three samples from the area between San Cristóbal and Cosigüina and the fourth from the southern flank of Cosigüina. A representative step-heating spectrum for sample C-06-Nic-13 is shown in Fig. 6.

The samples collected between the Coyoil and active volcanic fronts (Nic-00-2, Nic-00-1BM, and LS-00-4), have ⁴⁰Ar/³⁹Ar within the range of Tinajas and as well as similar La/Yb and U/Th values. For these reasons, they are considered to be part of the Tinajas unit.

Regardless of which samples are included as part of the Tinajas, it is important to note that between 1 and 2 Ma, there was active volcanism in El Salvador (samples Bal-8, and Bal-10; Table 1), Nicaragua, and Costa Rica where the Monteverde Formation was found to be 1.1–2.2 Ma (Carr et al., 2007).

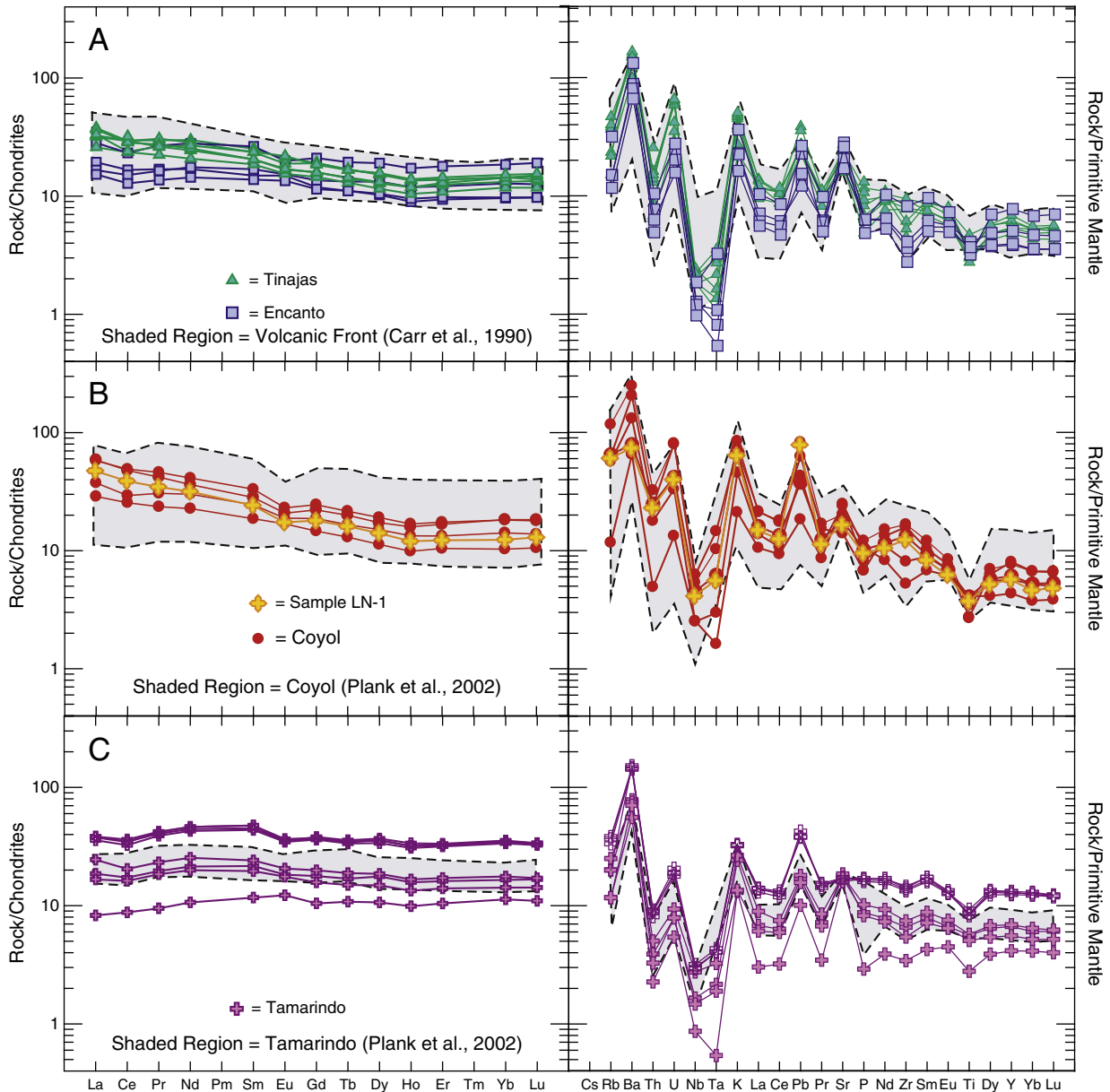


Fig. 4. Chondrite and primitive mantle normalized trace element patterns. A) Encanto and Tinajas units. B) Coyoil Group with sample LN-1 labeled. C) Tamarindo Formation.

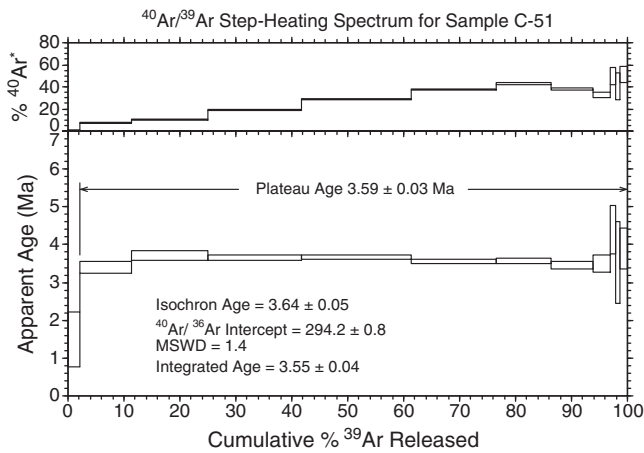


Fig. 5. Step heating spectrum for sample C-51.

5. Discussion

5.1. Variation in sediment input

The new data presented in this paper allowed a more detailed reconstruction of the evolution of volcanism in Nicaragua and fills a temporal gap where volcanic activity was thought to be absent (Plank et al., 2002).

The increase in U/Th values in Nicaraguan volcanic material since the Miocene has been attributed to changes in the subducting sediments following the “carbonate crash” (Plank et al., 2002) at 10 Ma. At that time, the Central American isthmus began to close, which shut off an important flow of water from the Caribbean to the Pacific (Coates et al., 1992; Farrell et al., 1995; Lyle et al., 1995). This caused the carbonate compensation depth to rise and sediments to become enriched in organic carbon at the expense of carbonate (Hoffmann et al., 1981). The result is that the Cocos plate sediments consist mainly of a lower carbonate layer and an upper hemipelagic layer, with the latter unit showing enrichment in U (Patino et al., 2000). This increase in uranium content of subducted sediments is reflected in Nicaraguan lavas in the form of a substantial increase in U/Th values between the Miocene and active volcanic front volcanism (Patino et al., 2000; Plank et al., 2002). The precise timing and rate of this increase could not be determined because there was a gap in the volcanic record between 7 Ma and 0.35 Ma (Carr et al., 2007). The data presented here reduce the length of this gap roughly by half,

leaving only the period between 7 and 3.6 Ma without known volcanism. Fig. 7 shows that the transition from low to high U/Th was more gradual than the data shown before the temporal gap in the record was reduced by the present data. Fig. 7 also shows that about half of the increase in U/Th happened by the end of Coyoil volcanism ~7 Ma, suggesting that the effects of the carbonate crash on volcanism had already begun. Given the limited number of samples collected from this time period, additional sampling is needed to pinpoint the exact timing of U/Th enrichment in the volcanic front.

If we assume that the subduction rate varied between 8 and 10 cm/yr since the Miocene, the slab dip varied between 45° and 84°, and the depth of melting generation was between 140 and 200 km (ranges from Carr et al., 1990; Protti et al., 1995), it would take 1.4–2.5 Ma for subducted sediments to reach the depth of melting. Given that flux-melted mantle can reach the surface in less than 8000 years (Clark et al., 1998), this process is essentially instantaneous for our purposes. Our data suggest a lag of between 1.1 and 3 Ma from the time of the carbonate crash to the first increases in the U/Th values of the erupted products. However, the carbonate crash was not a single moment in time, but rather a gradual transition. For this reason, it is difficult to predict exactly how long it would take for the sediments to build up sufficiently before they are thick enough to influence arc geochemistry. The range of subduction times calculated above (1.4–2.5 Ma), suggest that subducted sediment at the trench could reach the depth of melting over a 1.1 Ma time range. That range is plotted on Fig. 7, beginning 1.4 Ma after the carbonate crash. Further modeling of the rates of sedimentation and input would be required to refine the predicted age ranges provided here and in Fig. 7.

5.2. Origin of the Tamarindo Formation and the Nicaraguan Depression

The presence of Mid Miocene Tamarindo and Coyoil volcanism on either side of the Nicaraguan Depression has led some researchers to conclude that the two units were once connected and were later tectonically separated by normal faulting. In this view, the Tamarindo Formation and Coyoil Group are “fully equivalent” as Weyl (1980) concluded and the Nicaraguan Depression is a fault-bounded pull-apart basin as argued by Weinberg (1992). Key to this view is determining the depth of the sediment fill within the depression and the total amount of extension. Weyl (1980) cites a “personal communication” to place the depth at 2000 m and the maximum exposed fault displacement at 900 m, for a total displacement of almost 3 km. Weinberg provides the same depth estimate, also based on personal communication. However, after a closer examination, van Wyk de Vries (1993) found that the sediment fill in the Nicaraguan Depression is much thinner (only 150 m deep) than previously thought based on a well log from a geothermal plant near Momotombo Volcano. In addition, faults such as the Mateare were found to be local strike-slip features, which limited the possibility that the Nicaraguan Depression is a typical fault-graben system. Seismic data from the Tomography Under Costa Rica And Nicaragua (TUCAN) project (Mackenzie et al., 2008; Rychert et al., 2008; Syracuse et al., 2008) and gravity modeling (Elming and Rasmussen, 1997) have indicated the presence of thinner crust under Nicaragua and sediment thickness in the Nicaraguan Depression of 2–2.5 km. The most complete study of extension within the Nicaraguan Depression is by Funk et al. (2009) who use subsurface data to reveal a half-graben with the controlling normal faults on the western side. The sediment thickness increases westward across the depression to a maximum of 2000–3000 m.

Morgan et al. (2008), argue that the presence of Mid Miocene volcanics on either side of the Nicaraguan Depression suggests that large amounts of extension over the last 14 Ma are responsible for their separation. However, calculations by McKenzie (1978) suggest that the limited regional subsidence is not enough to accommodate the 80 km of extension that separates the Tamarindo from the Coyoil.

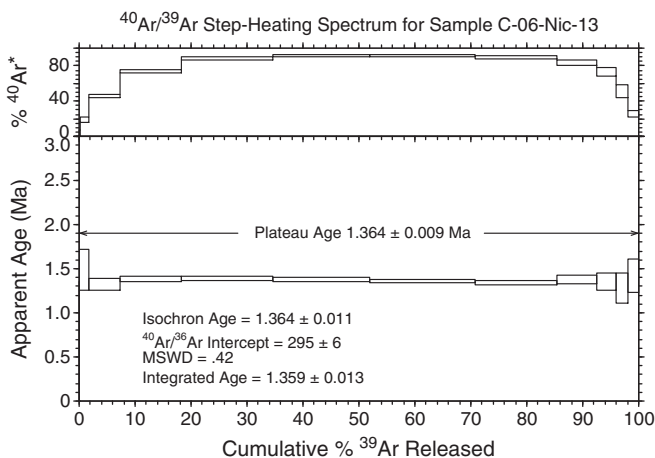


Fig. 6. Step heating spectrum for sample C-06-Nic-13.

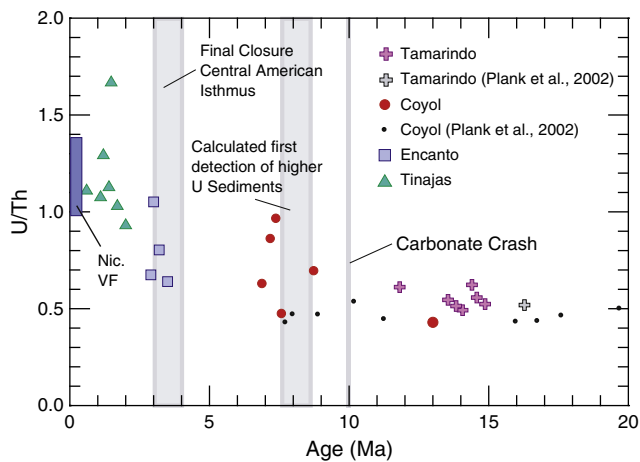


Fig. 7. U/Th values for all dated samples vs. age. Purple crosses are Tamarindo, blue squares are Encanto, green triangles are Tinajas, red circles are Coyoil Group, black dots are Coyoil from Plank et al. (2002), gray crosses are Tamarindo from Plank et al., 2002, and gray shaded regions are from Plank et al. (2002). Blue shaded region is active volcanic front (Carr et al., 1990).

To tectonically accomplish this would either require the formation of ocean crust to fill the gap or subsidence that far exceeds even the largest estimates of offset associated with the Nicaraguan Depression. The new data from Funk et al. (2009) do not show evidence of rifting on the scale required by Morgan et al. (2008) to tectonically separate the Tamarindo and Coyoil.

More importantly, data presented here suggest that although the Tamarindo Formation is coeval with Coyoil volcanism, it is geochemically distinct. First, the REE patterns of Miocene Coyoil samples are significantly steeper than Miocene Tamarindo samples (Fig. 4). Second, La/Yb values are higher for Tamarindo than Coyoil (Fig. 8). La/Yb values in Central American rocks have been used as a proxy for degree of mantle melting assuming that the source composition does not change significantly, with high values correlating to low degrees of melting and low values correlating to high degrees of melting (Carr et al., 1990).

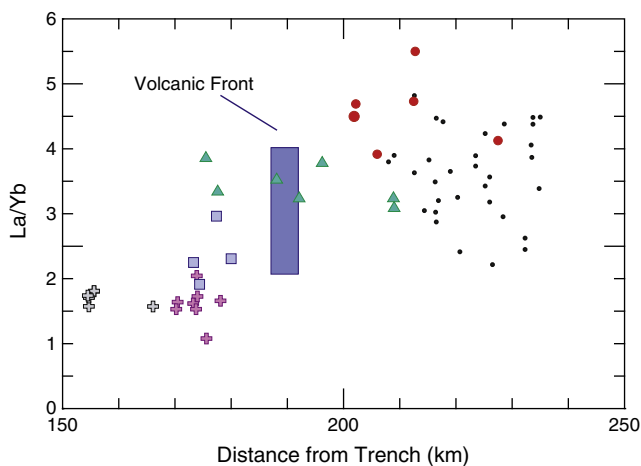


Fig. 8. La/Yb values vs. distance from trench. Purple crosses are Tamarindo, blue squares are Encanto, green triangles are Tinajas, red circles are Coyoil Group, black dots are Coyoil from Plank et al. (2002), and gray crosses are Tamarindo from Plank et al. (2002). Blue shaded region is active volcanic front (Carr et al., 1990).

6. Conclusions

- (1) Our new data reduces the duration of the Nicaraguan volcanic hiatus since the Miocene from a total of ~7 Ma to 3.6 Ma.
- (2) The increase in U/Th values between the Miocene and active arc was more gradual than previously thought and due to the carbonate crash brought on by the closure of the Central American isthmus.
- (3) The Tamarindo Formation was likely emplaced in situ and was not tectonically separated from the Coyoil Group.

Supplementary materials related to this article can be found online at doi:10.1016/j.jvolgeores.2011.02.002.

Acknowledgment

We would like to thank Keystone College and the Department of Earth and Planetary Sciences at Rutgers University for their support. This initiative was also supported by the National Science Foundation (grant EAR0203388), the Postdoctoral Research Fellowship in Earth, Environmental, and Ocean Sciences from Lamont-Doherty Earth Observatory, and the Department of Earth and Environmental Sciences at Columbia University to E. Gazel. This is a Lamont-Doherty contribution No. 7453. The manuscript benefited greatly from comments and suggestions offered by Tom Vogel, Terry Plank, Luca Ferrari, Jim Walker, and Kaj Hoernle.

References

- Carr, M.J., 1984. Symmetrical and segmented variation of physical and geochemical characteristics of the Central American volcanic front. *J. Volcanol. Geoth. Res.* 20, 231–252.
- Carr, M.J., Feigenson, M.D., Bennett, E.A., 1990. Incompatible element and isotopic evidence for tectonic control of source mixing and melt extraction along the Central American arc. *Contrib. Mineral. Petrol.* 105, 369–380.
- Carr, M.J., Saginor, I., Alvarado, G.E., Bolge, L.L., Lindsay, F.N., Milidakis, K., Turrin, B.D., Feigenson, M.D., Swisher III, C.C., 2007. Element fluxes from the volcanic front of Nicaragua and Costa Rica. *Geochim. Geophys. Res.* 12, 1525–1527.
- Clark, S.K., Reagan, M.K., Plank, T., 1998. Trace element and U-series systematics for 1963–1965 tephra from Irazú Volcano, Costa Rica: implications for magma generation processes and transit times. *Geochim. Cosmochim. Acta* 62 (15), 2689–2699.
- Coates, A.G., Jackson, J.B.C., Collins, L.S., Cronin, T.M., Dowsett, H.J., Bybell, L.M., Jung, P., Obando, J.A., 1992. Closure of the Isthmus of Panama; the near-shore marine record of Costa Rica and western Panama. *Bull. Geol. Soc. Am.* 104 (7), 814–828.
- Criss, J., 1980. Fundamental parameters calculations on a laboratory microcomputer. *Advances in X-Ray Analysis* 23, 93–97.
- Darce, M., 1989. Mineralogical alteration patterns, chemical mobility and origin of the La Libertad Gold Deposits, Nicaragua. Ph.D. Thesis, University of Stockholm, Sweden.
- Deino, A., Tauxe, L., Monaghan, M., Hill, A., 2002. $^{40}\text{Ar}/^{39}\text{Ar}$ geochronology and paleomagnetic stratigraphy of the Lukeino and lower Chemeron Formations at Tabarin and Kapcheberek, Tugen Hills, Kenya. *J. Hum. Evol.* 42, 117–140.
- Demets, C., 2001. A new estimate for present-day Cocos–Caribbean plate motion: implications for slip along the Central American Volcanic Arc. *Geophys. Res. Lett.* 28 (21), 4043–4046.
- Dengo, G., 1968. Estructura geológica, historia tectónica, y morfología de América Central. Centro Regional de ayuda técnica, México, pp. 1–50.
- Ehrenborg, J., 1996. A new stratigraphy for the Tertiary volcanic rocks of the Nicaraguan highland. *Geol. Soc. Am. Bull.* 108, 830–842.
- Elming, S.A., Rasmussen, T., 1997. Results of magnetotelluric and gravimetric measurements in western Nicaragua, Central America. *Geophys. J. Int.* 128, 647–658.
- Elming, S.A., Lauer, P., Ubieta, K., 2001. A paleomagnetic study of Tertiary rocks in Nicaragua, Central America. *Geophys. J. Int.* 147, 294–309.
- Farrell, J., Raffi, I., Janacek, T.R., Murray, D.W., Levitan, M., Dadey, K.A., Emeis, K.-C., Lyle, M., Flores, J.-A., Hovan, S., 1995. Late Neogene sedimentation, patterns, in the eastern equatorial Pacific Ocean. In: Pisias, N.G., Mayer, L.A., Janacek, T.R., van Andel, T.H. (Eds.), *Proceedings of the Ocean Drilling Program, Scientific Results*, 138, pp. 717–753.
- Funk, Juston, Mann, Paul, McIntosh, Kirk, Stephens, Jason, 2009. Cenozoic tectonics of the Nicaraguan depression, Nicaragua, and Median Trough, El Salvador, based on seismic-reflection profiling and remote-sensing data. *GSA Bull.* 121 (11/12), 1491–1521 November/December 2009.
- Hannah, R., Vogel, T., Patino, L., Alvarado, G., Pérez, W., Smith, D., 2002. Origin of silicic volcanic rocks in Central Costa Rica: a study of a chemically variable ash-flow sheet in the Tiribí Tuff. *Bull. Volcanol.* 64, 117–133.

- Hoffmann, E.E., Buslacchi, A.J., O'Brien, J.J., 1981. Wind generation of the Costa Rica Dome. *Science* 214, 552–554.
- Lyle, M., Dadey, K.A., Farrell, J.W., 1995. The Late Miocene (11–8 Ma) Eastern Pacific carbonate crash: evidence for reorganization of deep-water circulation by the closure of the Panama Gateway. In: Piasias, N.G., Mayer, L.A., Janecek, T.R., van Andel, T.H. (Eds.), *Proceedings of the Ocean Drilling Program, Scientific Results*, 138, pp. 821–838.
- Mackenzie, L., Abers, G., Fisher, K., Syracuse, E., Protti, M., Gonzalez, V., Strauch, W., 2008. Crustal structure along the southern Central American volcanic front. *Geochem. Geophys. Geosyst.* 9 (8), 1–19.
- McBirney, A., Williams, H., 1965. Volcanic history of Nicaragua. *Univ. Calif. Publ. Geol. Sci.* 55, 1–73.
- McKenzie, D., 1978. Some remarks on the development of sedimentary basins. *Earth Planet. Sci. Lett.* 40, 25–32.
- Morgan, J., Ranero, C.R., Vannucchi, P., 2008. Intra arc extension in Central America: links between plate motions, tectonics, volcanism, and geochemistry. *Earth Planet. Sci. Lett.* 272, 365–371.
- Nystrom, J., Levy, B., Troeng, B., Ehrenborg, J., Carranza, G., 1988. Geochemistry of volcanic rocks in a traverse through Nicaragua. *Revista Geol. Am. Cent.* 8, 77–109.
- Patino, L.C., Carr, M.J., Feigenson, M.D., 2000. Local and regional variations in Central American arc lavas controlled by variations in subducted sediment input. *Contrib. Mineral. Petrol.* 138, 265–283.
- Peccerillo, R., Taylor, S.R., 1976. Geochemistry of Eocene calc-alkaline rocks from the Kastamonu Area, Northern Turkey. *Contrib. Mineral. Petrol.* 58, 63–81.
- Plank, T., Balzer, V., Carr, M.J., 2002. Nicaraguan volcanoes record paleoceanographic changes accompanying closure of the Panama Gateway. *Geology* 30, 1087–1090.
- Protti, M., Guendel, F., McNally, K., 1995. Correlation between the age of the subducting Cocos Plate and the geometry of the Wadati–Beniof zone under Nicaragua and Costa Rica. In: Mann, P. (Ed.), *Geologic and tectonic development of the Caribbean Plate boundary in southern Central America: Geol SocAm (Special Paper)*, 295, pp. 309–326.
- Renne, P.R., Swisher, C.C., Deino, A.L., Karner, D.B., Owens, T.L., DePaolo, D.J., 1998. Intercalibration of standards, absolute ages and uncertainties in $^{40}\text{Ar}/^{39}\text{Ar}$ dating. *Chem. Geol.* 145, 117–152.
- Rychert, C., Fisher, K., Abers, G., Plank, T., Syracuse, E., Protti, M., Gonzalez, V., Strauch, W., 2008. Strong along-arc variations in the mantle wedge beneath Costa Rica and Nicaragua. *Geochem. Geophys. Geosyst.* 9 (10), 1–26.
- Syracuse, E., Abers, G., Fisher, K., Mackenzie, L., Rychert, C., Protti, M., Gonzalez, V., Strauch, W., 2008. Seismic tomography and earthquake locations in the Nicaraguan and Costa Rican upper mantle. *Geochem. Geophys. Geosyst.* 9.
- Szymanski, D.W., 2007. Magmatic evolution of ignimbrites in the Bagaces Formation, Guanacaste Province, Costa Rica. Ph.D. Thesis, Michigan State University, 1–340.
- Turrin, B.D., Donnelly-Nolan, J.M., Hearn Jr., B.C., 1994. $^{40}\text{Ar}/^{39}\text{Ar}$ ages from the rhyolite of Alder Creek, California; age of the Cobb Mountain normal-polarity subchron revisited. *Geology* 22–3, 251–254.
- van Wyk de Vries, B., 1993. Tectonics and magma evolution of Nicaraguan volcanic systems. Ph.D. Thesis, Open University, Milton Keynes, UK, 1–328.
- Weinberg, R.F., 1992. Neotectonic development of Western Nicaragua. *Tectonics* 11 (5), 1010–1017.
- Weyl, R., 1980. Geology of Central America. *Beitr. Region. Geol. Erde* 15, 1–371.